Adsorption and Oxidation of Propane and Cyclopropane on $IrO_2(110)$

Journal:	*Physical Chemistry Chemical Physics*
Manuscript ID	CP-ART-09-2018-006125.R1
Article Type:	Paper
Date Submitted by the Author:	27-Oct-2018

Complete List of Authors:	Martin, Rachel; University of Florida, Department of Chemical Engineering Kim, Minkyu; The Ohio State University, William G Lowrie Department of Biomolecular and Chemical Engineering Franklin, Austin; University of Florida, Department of Chemical Engineering Bian, Yingxue; University of Florida, Department of Chemical Engineering Asthagiri, Aravind; The Ohio State University, William G Lowrie Department of Biomolecular and Chemical Engineering Weaver, Jason; University of Florida, Department of Chemical Engineering

Adsorption and Oxidation of Propane and Cyclopropane on $IrO_2(110)$

Rachel Martin,[1,†] Minkyu Kim,[2,†] Austin Franklin,[1] Yingxue Bian,[1] Aravind Asthagiri[2] and Jason F. Weaver[1]

[1]Department of Chemical Engineering, University of Florida, Gainesville, FL 32611, USA

[2]William G. Lowrie Chemical & Biomolecular Engineering, The Ohio State University, Columbus, OH 43210, USA

† Rachel Martin and Minkyu Kim contributed equally to this work.

*To whom correspondence should be addressed, weaver@che.ufl.edu

Tel. 352-392-0869, Fax. 352-392-9513

Abstract

We investigated the adsorption and oxidation of *n*-propane and cyclopropane (C_3H_8 and c-C_3H_6) on the IrO_2(110) surface using temperature programmed reaction spectroscopy (TPRS) and density functional theory (DFT) calculations. We find that the activation of both C_3H_8 and c-C_3H_6 is facile on IrO_2(110) at low temperature, and that the dissociated alkanes oxidize during TPRS to produce CO, CO_2 and H_2O above ~400 K. Propane conversion to propylene is negligible during TPRS for the conditions studied. Our results show that the maximum yield of alkane that oxidizes during TPRS is higher for c-C_3H_6 compared with C_3H_8 (~0.30 vs. 0.18 monolayer) and that pre-hydrogenation of the surface suppresses c-C_3H_6 oxidation to a lesser extent than C_3H_8. Consistent with the experimental results, DFT predicts that C_3H_8 and c-C_3H_6 form σ-complexes on IrO_2(110) and that C-H bond activation of the complexes as well as subsequent dehydrogenation are highly facile via H-transfer to O_{br} atoms (bridging O-atoms). Our calculations predict that propane conversion to gaseous propylene is kinetically disfavored on IrO_2(110) because HO_{br} recombination makes O_{br} atoms available to promote further dehydrogenation at lower temperatures than those needed for the adsorbed C_3H_6 intermediate to desorb as propylene. We also present evidence that that the ability for c-C_3H_6 to activate via ring-opening is responsible for cyclopropane attaining higher reaction yields during TPRS and exhibiting a weaker sensitivity to surface pre-hydrogenation compared with n-propane.

Introduction

Developing catalysts that can directly convert light alkanes to olefins is gaining increasing interest due to the need to better utilize abundant hydrocarbon resources, particularly shale gas. The non-oxidative steam cracking of ethane and propane produces ethylene and propylene, respectively, in high yields but is energy intensive and suffers from high capital costs and coking. The oxidative dehydrogenation (ODH) of ethane and propane occurs in the presence of oxygen and produces the olefin while the released hydrogen is concurrently oxidized to water. Advantages of the ODH of alkanes are that high conversion is thermodynamically favored at low temperature because the reaction is exothermic and coking is mitigated by oxygen in the feed stream. Various metal oxides as well as alkali chlorides are effective in promoting the ODH of ethane and propane, with VO_x-based catalysts exhibiting the most favorable performance.[1-10] However, the catalysts that have been investigated to date do not achieve sufficient activity and selectivity to be utilized at the industrial scale.

Initial C-H bond activation is typically the rate-controlling step in the catalytic processing of light alkanes. This situation creates challenges for developing efficient catalysts that promote the ODH of ethane and propane, while limiting extensive oxidation to CO and CO_2 due to the need to operate at elevated temperature to initiate reaction. We have recently shown that the initial C-H bond cleavage of methane and ethane is highly facile on the $IrO_2(110)$ surface and that subsequent reaction steps control the rate of conversion of these light alkanes to gaseous products.[11, 12] We specifically find that the initial C-H bond cleavage of CH_4 and C_2H_6 occurs on $IrO_2(110)$ at temperatures as low as 150 K, and that extensive oxidation of the hydrocarbon fragments to CO_x species initiates at higher temperatures (>~ 400 K) during temperature programmed reaction spectroscopy (TPRS). We also find that ethane dehydrogenates on $IrO_2(110)$ to produce ethylene,

with C_2H_4 desorption initiating at 350 K during TPRS and nearly 40% of the dissociated ethane transforming to ethylene at high ethane coverage.[11] Our results show that the ethylene selectivity can be enhanced by hydrogenating a fraction of the O_{br} atoms prior to ethane adsorption. On the pre-hydrogenated surface, the adsorbed ethylene intermediate resulting from partial ethane dehydrogenation has a high probability of being surrounded by inactive HO_{br} groups and will thus desorb as C_2H_4 rather than further dehydrogenating. The ability to achieve facile initial C-H bond activation on $IrO_2(110)$ and also enhance the partial oxidation selectivity of this surface may provide opportunities to develop IrO_2-based catalysts that can efficiently and selectivity convert light alkanes to value-added products.

In the present study, we investigated the adsorption and oxidation of propane and cyclopropane (C_3H_8 and c-C_3H_6) on $IrO_2(110)$ using TPRS experiments and density functional theory (DFT) calculations. We find that both propane compounds undergo facile activation on $IrO_2(110)$ at low temperature, and that the resulting hydrocarbon fragments undergo only extensive oxidation to CO_x species during TPRS. Propane conversion to gaseous propylene is negligible under all conditions studied, including on pre-hydrogenated $IrO_2(110)$. Our DFT calculations predict that the lack of propylene evolution results from a high stability of the adsorbed propylene intermediate relative to HO_{br} groups. We also present evidence that that the ability for c-C_3H_6 to activate via ring-opening enhances the reactivity of cyclopropane relative to n-propane on both clean and pre-hydrogenated $IrO_2(110)$. Overall, the present study clarifies factors that influence the activity and selectivity of the $IrO_2(110)$ surface in promoting alkane oxidation.

Experimental Details

Details of the UHV analysis chamber with an isolatable ambient-pressure reaction cell utilized in the present study have been reported previously.[11] Briefly, the Ir(100) crystal employed in this study is a circular disk (9 mm × 1 mm) that is attached to a liquid-nitrogen-cooled, copper sample holder by 0.015" W wires that are secured to the edge of crystal. A type K thermocouple was spot welded to the backside of the crystal for temperature measurements. Resistive heating, controlled using a PID controller that varies the output of a programmable DC power supply, supports linearly ramping from 80 to 1400 K and maintaining the sample temperature. Sample cleaning consisted of cycles of Ar^+ sputtering (2000 eV, 1.5 μA) at 1000 K, followed by annealing at 1400 K for several minutes. The sample was subsequently exposed to 5×10^{-7} Torr of O_2 at 900 K for several minutes to remove surface carbon, followed by flashing to 1400 K to remove final traces of oxygen. We considered the Ir(100) sample to be clean when we obtained sharp low-energy electron diffraction (LEED) patterns consistent with the reconstructed (5 × 1) structure and did not detect impurities using AES and detected negligible CO and CO_2 production during flash desorption after adsorbing oxygen.

We generated an IrO_2(110) film by exposing Ir(100) to 5 Torr O_2 (Airgas, 99.999%) for a duration of 10 minutes (3×10^9 Langmuir) in the ambient-pressure reaction cell at a surface temperature of 775 K. Our ambient-pressure reaction cell is designed to reach elevated gas pressure while maintaining UHV in the analysis chamber.[11] After preparation of the oxide film, we lowered the surface temperature to 600 K, and then evacuated O_2 from the reaction cell and transferred the sample back to the UHV analysis chamber. We exposed the film to ~23 L O_2 while cycling the surface temperature between 300 and 650 K to fill oxygen vacancies that may have been created during sample transfer from the reaction cell to the analysis chamber. This procedure produces a

high-quality $IrO_2(110)$ surface that has a stoichiometric surface termination and consists of ~10 layers of $IrO_2(110)$, corresponding to a thickness of 3.2 nm.

The $IrO_2(110)$ surface unit cell is rectangular, with bulk-terminated dimensions of a = 3.16 Å and b = 6.36 Å, and the surface consists of alternating rows of Ir_{cus} and O_{br} atoms along the [001] direction (see Figure S1, Supporting Information). Each of these surface species has a single dangling bond due to the decrease in bond coordination relative to bulk IrO_2. On the basis of the $IrO_2(110)$ unit cell, the areal density of Ir_{cus} atoms and O_{br} atoms is equal to 37% of the Ir(100) surface atom density of 1.36×10^{15} cm^2. Since Ir_{cus} atoms are active adsorption sites, we define 1 ML as equal to the density of Ir_{cus} atoms on the $IrO_2(110)$ surface.

We investigated the adsorption and reactivity of C_3H_8 and c-C_3H_6 (Airgas, 99.999%) on the s-$IrO_2(110)$ surface using TPRS. We note that a small quantity of H_2 (~0.1 to 0.2 ML) adsorbs on the as-prepared $IrO_2(110)$ films during cooling to 90 K, prior to alkane adsorption. After an alkane exposure, we positioned the sample in front of a shielded mass spectrometer at a distance of ~5 mm and heated at a constant rate of 1 K/s. In most cases we terminated the TPRS experiments at 650 K, because we find that this final temperature represents an optimal balance between desorbing nearly all of the H_2O product and the ability to conveniently regenerate a clean $IrO_2(110)$ surface in UHV to allow repeated TPRS experiments. As shown below, heating to 650 K is sufficient to completely desorb all of the carbon-containing products but terminates the experiment within the trailing edge of the H_2O TPRS feature (see below). We estimate that ~0.04 to 0.08 ML of H-atoms remains on the surface at 650 K, depending on the initial alkane coverage. After each TPRS experiment, we expose the surface to ~23 L of O_2 while heating between 300 and 650 K to remove the residual hydrogen and also eliminate oxygen-vacancies that are created during alkane oxidation. Reproducibility in our TPRS results demonstrates that this O_2 treatment in UHV is effective in

regenerating the clean $IrO_2(110)$ surface. In selected cases, we discontinued the TPRS experiment at a final temperature of 800 K to capture the entire H_2O TPRS feature. We find, however, that subsequent O_2 treatment in UHV is insufficient to fully restore the oxide surface after heating to 800 K. Initially, we monitored a wide range of desorbing species to identify the main products that are generated from reactions of propane and cyclopropane on $IrO_2(110)$, and found that the only desorbing species are C_3H_8 or c-C_3H_6, CO, CO_2, and H_2O. We quantified desorption yields using established procedures as described in the Supporting Information (SI).

We also used TPRS to investigate the adsorption and reactivity of propane and cyclopropane on hydrogen pre-saturated $IrO_2(110)$. We prepared the H pre-saturated surfaces by adsorbing H_2 to saturation at 90 K, followed by heating to 380 K to promote H-atom migration from Ir_{cus} to O_{br} atoms. In a previous study, we reported that H_2 dissociates efficiently on $IrO_2(110)$ at 90 K to produce pairs of H_{ot} and HO_{br} species and that H_2 saturates the $IrO_2(110)$ surface at a coverage of ~0.67 ML at 90 K.[13] We further reported evidence that subsequent heating to 380 K promotes the migration of H-atoms from Ir_{cus} to O_{br} sites, and estimate that this treatment causes a redistribution of the surface H-atoms such that the surface contains ~0.5 ML of H_{ot} atoms and 0.8 ML of HO_{br} groups after H_2 saturation at 90 K.

Computational Details

All plane wave DFT calculations were performed using the projector augmented wave pseudopotentials[14] provided in the Vienna ab initio simulation package (VASP).[15, 16] The Perdew-Burke-Ernzerhof (PBE) exchange-correlation functional[17] was used with a plane wave expansion cutoff of 450 eV. Dispersion interactions are modeled using the DFT-D3 method developed by

Grimme et al.[18] We used four layers to model the $IrO_2(110)$ film which is an ~12 Å thick slab. The lateral dimensions of the slab are fixed to the PBE bulk lattice constant of IrO_2 (a = 4.54 Å and c = 3.19 Å). The bottom two layers are fixed, but all other lattice atoms are allowed to relax during the calculations until the forces are less than 0.05 eV/Å. A vacuum spacing of ~25 Å was included, which is sufficient to reduce the periodic interaction in the surface normal direction. In terms of system size, a 2×4 unit cell with a corresponding $2 \times 2 \times 1$ Monkhorst-Pack k-point mesh is employed. Unless otherwise noted, our DFT calculations were performed for a single C_3H_8 molecule adsorbed within the 2×4 surface model of $IrO_2(110)$, and corresponds to a C_3H_8 coverage equal to 12.5% of the total density of Ir_{cus} atoms and 25% of the Ir_{cus} density within one Ir_{cus} row. In the present study, we define the binding energy, E_b, of an adsorbed C_3H_8 molecule on the surface using the expression,

$$E_b = \left(E_{C_3H_8} + E_{surf}\right) - E_{C_3H_8 + surf}$$

where $E_{C_3H_8 + surf}$ is the energy of C_3H_8 on the bare surface, E_{surf} is the energy of the bare surface, and $E_{C_3H_8}$ is the energy of an isolated C_3H_8 molecule in the gas phase. All reported binding energies are corrected for zero-point vibrational energy. From the equation above, a large positive value for the binding energy indicates a high stability of the adsorbed C_3H_8 molecule under consideration. We evaluated the barriers for C_3H_8 oxidation on the $IrO_2(110)$ surface using the climbing nudged elastic band (cNEB) method and confirmed that the resulting transition states have one imaginary vibrational frequency.[19]

Experimental Results

TPRS of C_3H_8 adsorbed on IrO_2(110)

Our TPRS results show that the IrO_2(110) surface is highly reactive toward *n*-propane as nearly all of the adsorbed C_3H_8 oxidizes to CO, CO_2 and H_2O during TPRS at low initial C_3H_8 coverages (<~ 0.2 ML) (Figure 1a). The CO_2 and CO products desorb in TPRS peaks centered at 535 and 565 K, while H_2O desorbs in a broader feature that initiates at ~400 K and extends to at least 650 K. As discussed in Experimental Details, the H_2O TPRS feature shown in Figure 1a remains above the baseline at 650 K when the experiment was terminated. We also observe a small C_3H_8 desorption peak at ~125 K that likely arises from weakly-bound *n*-propane on a minority surface phase or kinetically-trapped in a meta-stable configuration on IrO_2(110). The CO_2, CO and H_2O TPRS peaks intensify and reach saturation as the propane coverage increases to just above ~0.20 ML, while the small propane TPRS peak near 125 K increases marginally.

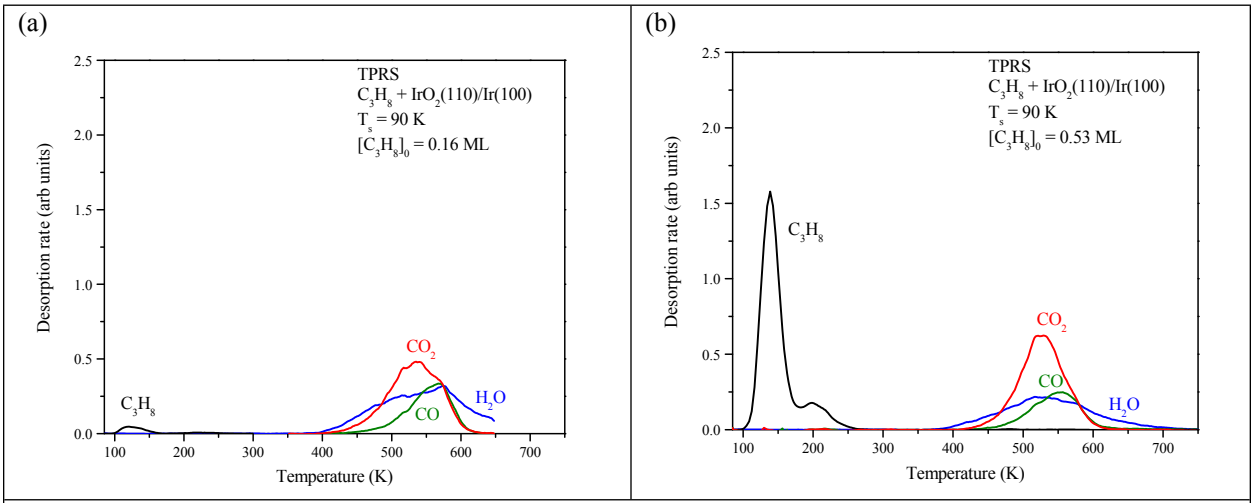

Figure 1. TPRS spectra of C_3H_8, CO, CO_2 and H_2O obtained after adsorbing C_3H_8 on IrO_2(110) at 90 K to reach initial C_3H_8 coverages of (a) 0.16 ML and (b) 0.53 ML.

We find that propane TPRS peaks develop below ~260 K after the oxidation products attain maximum yields, and observe only CO, CO_2 and H_2O as reaction products up to high propane

coverage. A C_3H_8 desorption peak at 205 K emerges initially and nearly saturates, before a peak at 155 K becomes evident just above ~0.30 ML (see Fig. S2 in the SI) and downshifts to ~140 K as this peak intensifies with increasing propane coverage. Consistent with prior studies,[11, 12] we attribute the TPRS peak at 205 K to C_3H_8 σ-complexes adsorbed on the Ir_{cus} rows while the peak at ~140-155 K is consistent with propane associated with O_{br} sites. At the highest *n*-propane coverage studied (~0.58 ML), the C_3H_8 TPRS spectrum exhibits an intense peak at 140 K with a small shoulder on the leading edge and a smaller peak at 205 K attributed to C_3H_8 σ-complexes (Figure 1b). Using Redhead analysis with a maximum value of the desorption pre-factor (2×10^{19} s^{-1}),[20] we estimate a binding energy of 79 kJ/mol for the propane TPRS peak at 205 K. Prior studies show that maximum pre-factors are appropriate for describing the desorption of *n*-alkane σ-complexes from TiO_2(110) and RuO_2(110).[21-23] We estimate that propane saturates the σ-complex state on IrO_2(110) at a coverage of about 0.25 ML, based on the amount of propane that desorbs above ~175 K plus the amount that reacts. This value agrees well with the saturation coverage reported for propane σ-complexes in a compressed layer on RuO_2(110).[22] Since the propane σ-complexes act as precursors for dissociation, our results show that initial C-H bond cleavage occurs at temperatures below 250 K during TPRS, i.e., before the σ-complexes completely desorb.

We find that propane conversion to propylene occurs negligibly during TPRS under the conditions studied. In contrast, we have recently reported that ethane dehydrogenates to ethylene on IrO_2(110) after the oxidation products attain maximum yields at moderate to high ethane coverage.[12] Nearly 40% of the reacted ethane evolves as ethylene at saturation of the C_2H_6 σ-complex state. Below, we present evidence that the stability of the partially-dehydrogenated hydrocarbon intermediates plays a decisive role in controlling the selectivity for alkane dehydrogenation to alkenes vs. extensive oxidation.

General mechanism for ethane and propane dehydrogenation on IrO_2(110)

It is instructive to briefly review the mechanism for alkane dehydrogenation on IrO_2(110), and the effects of surface hydrogenation. The general reaction steps for propane activation and subsequent dehydrogenation on IrO_2(110) may be represented by the following,

Initial C_3H_8 dissociation vs. desorption: $C_3H_8(ad) \rightarrow C_3H_8(g)$

$C_3H_8(ad) + O_{br} \rightarrow C_3H_7(ad) + HO_{br}$

C_3H_7 dehydrogenation: $C_3H_7(ad) + O_{br} \rightarrow C_3H_6(ad) + HO_{br}$

C_3H_6 dehydrogenation vs. desorption: $C_3H_6(ad) + O_{br} \rightarrow C_3H_5(ad) + HO_{br}$

$C_3H_6(ad) \rightarrow C_3H_6(g)$

Propane initially adsorbs in a molecular state C_3H_8(ad) and forms a σ-complex by datively bonding with Ir_{cus} atoms, and a competition between dissociation and desorption of the C_3H_8(ad) species determines the net probability of initial C-H bond cleavage. We have previously shown that ethane C-H bond cleavage as well as subsequent dehydrogenation on IrO_2(110) occurs by H-transfer to O_{br} atoms, and that HO_{br} groups are effectively inactive as H-atom acceptors.[12] Consistent with this finding, our TPRS results show that dissociation of the C_3H_8(ad) species is strongly favored over desorption at low C_3H_8 coverages when O_{br} atoms are available in high concentrations. Our results further suggest that the conversion of O_{br} atoms to HO_{br} groups is mainly responsible for C_3H_8 dissociation reaching saturation during TPRS beyond a critical C_3H_8 coverage.

After initial dissociation, the resulting C_3H_7(ad) species can dehydrogenate to C_3H_6(ad) species, and the C_3H_6(ad) species can further dehydrogenate via H-atom transfer to an O_{br} atom or, in principle, desorb as propylene. Again, the coverage of O_{br} atoms decreases with increasing initial C_3H_8 coverage because an increasing fraction of the O_{br} atoms is converted to HO_{br} groups via

dehydrogenation of the C_3H_8-derived species. According to the proposed reaction steps, C_3H_6 desorption could become favored as the O_{br} atom coverage decreases. In support of this idea, we have recently shown that hydrogenating a fraction of the O_{br} atoms prior to ethane adsorption enhances ethylene production on $IrO_2(110)$.[12] In this case, HO_{br} groups are effective in enhancing the ethylene selectivity because the barrier for ethylene desorption from $IrO_2(110)$ is lower than the barriers for O_{br} regeneration via adjacent HO_{br} recombination and H_2O desorption (~185 vs. 220-260 kJ/mol).[12, 13] As we show below, the barriers for gaseous propylene evolution are higher than those for HO_{br} recombination. As a result, extensive oxidation of propane is favored on $IrO_2(110)$ even at high, initial HO_{br} coverages, because O_{br} atoms become available at temperatures lower than those needed for propylene to desorb.

TPRS of cyclopropane (c-C_3H_6) adsorbed on $IrO_2(110)$

Figures 2a and 2b show TPRS results obtained after adsorbing representative low and high coverages of c-C_3H_6 on $IrO_2(110)$ at 90 K. At low initial coverages (<~ 0.20 ML), the reactivity of c-C_3H_6 is similar to that of C_3H_8 in that nearly all of the adsorbed c-C_3H_6 dissociates and extensively oxidizes above 400 K during TPRS (Figure 2a). The CO, CO_2 and H_2O TPRS peaks resulting from c-C_3H_6 and C_3H_8 oxidation are nominally identical, suggesting that a common reaction step(s), such as HO_{br} recombination to H_2O, controls the rate of extensive oxidation of alkane-derived intermediates on $IrO_2(110)$. Similar to ethane and *n*-propane, we observe a small c-C_3H_6 TPRS peak at ~130 K that likely arises from c-C_3H_6 adsorbed on a minority surface phase or a small amount of c-C_3H_6 that is kinetically-trapped on $IrO_2(110)$.

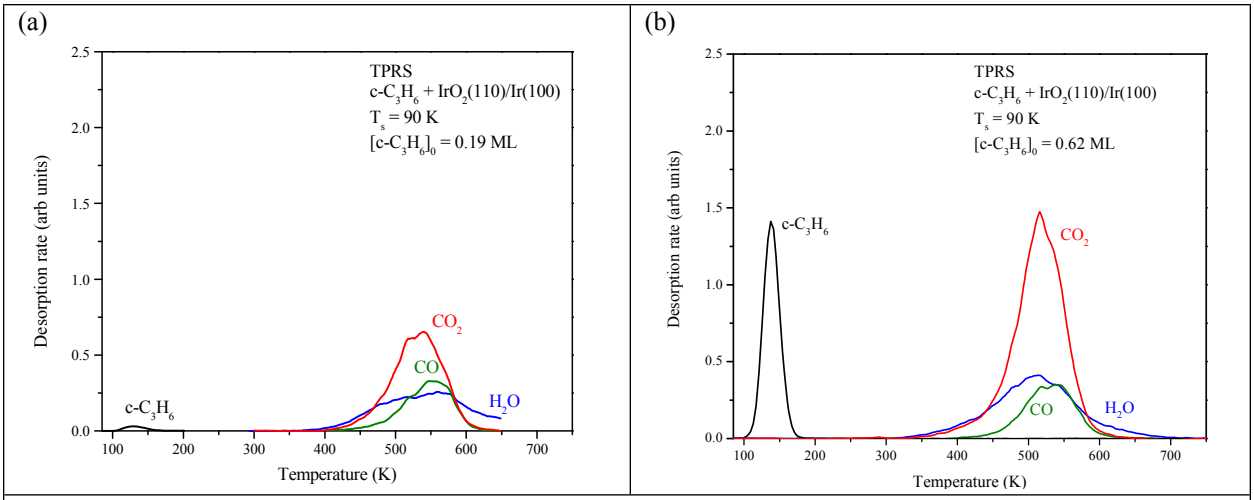

Figure 2. TPRS spectra of c-C_3H_6, CO, CO_2 and H_2O obtained after adsorbing c-C_3H_6 on IrO_2(110) at 90 K to reach initial c-C_3H_6 coverages of (a) 0.19 ML and (b) 0.62 ML.

The TPRS traces obtained at initial coverages above ~0.20 ML exhibit two main differences for c-C_3H_6 vs. C_3H_8 on IrO_2(110). First, c-C_3H_6 continues to extensively oxidize with increasing c-C_3H_6 coverage to above ~0.30 ML, producing CO and CO_2 TPRS peaks that are more intense than those resulting from C_3H_8 oxidation (Figure 2b vs. 1b). Additionally, we observe the development of only a single c-C_3H_6 TPRS peak at ~140 K as the oxidation products attain maximum yields above ~0.30 ML, with this peak intensifying with increasing c-C_3H_6 coverage to at least 0.70 ML. Using Redhead analysis, we estimate that the binding energy associated with the c-C_3H_6 TPRS peak at 140 K ranges from 40 to 50 kJ/mol.

The c-C_3H_6 TPRS spectra differ qualitatively from those of ethane and propane on IrO_2(110). Specifically, the TPRS spectra of ethane and propane exhibit a distinct feature from σ-complexes at 185 and 205 K, respectively, followed by the growth of a peak at lower temperature (~125, 140 K) that continues to intensify with increasing coverage to at least ~0.6 ML. The latter peak observed for ethane and propane behaves analogously to the single c-C_3H_6 TPRS peak that is evident in Figure 2b. We thus attribute the c-C_3H_6 TPRS peak at 140 K to weakly-bound c-C_3H_6

associated with O_{br} atoms. We conclude that c-C_3H_6 σ-complexes do form on IrO_2(110) in high coverages but that all of the complexes react rather than desorbing during TPRS and that a distinct TPRS feature from c-C_3H_6 σ-complexes is absent as a result. We present DFT results below that support this interpretation.

Product yields as a function of the C_3H_8 and c-C_3H_6 coverage

Figures 3a and 3b show estimates of the initial and oxidized TPRS yields of C_3H_8 and c-C_3H_6 σ-complexes on IrO_2(110) as a function of the total alkane coverage. We also plot the total alkane coverage to facilitate comparison with the product yields. We set the oxidized yield of the propane species equal to one third of the yield of CO + CO_2, where the factor of 1/3 converts the CO_x yield to the amount of C_3H_8 or c-C_3H_6 that oxidizes, and we define the initial amount of C_3H_8 σ-complexes as equal to the oxidized C_3H_8 yield plus the amount of C_3H_8 that desorbs in the TPRS feature at ~205 K. We assume that the initial coverage of c-C_3H_6 σ-complexes is equal to the oxidized yield for the reasons discussed above.

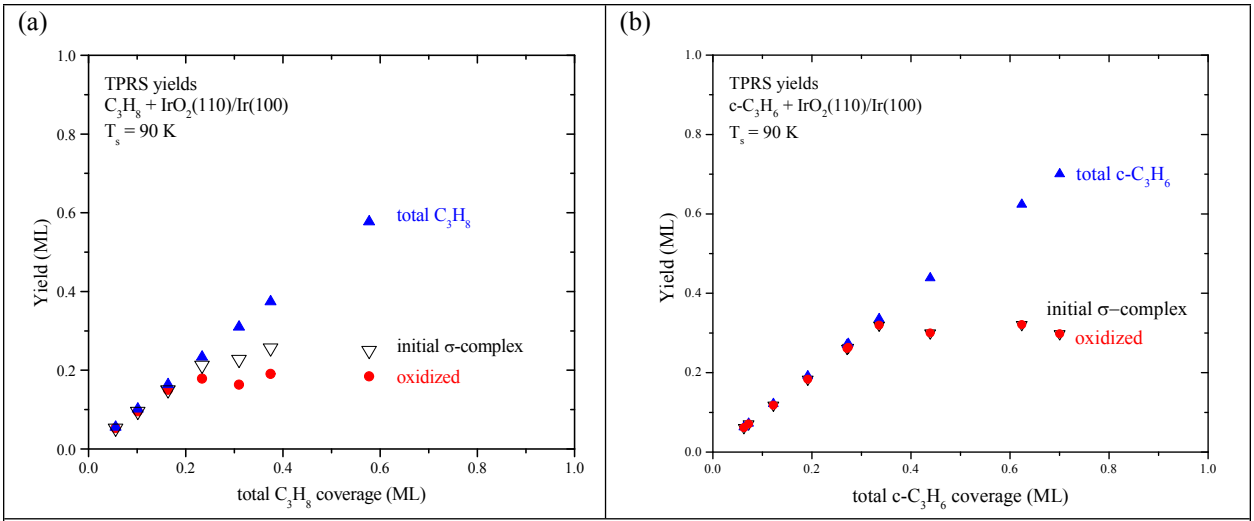

Figure 3. TPRS product yields as a function of the initial coverage of a) C_3H_8 adsorbed on $IrO_2(110)$ at 90 K, including the initial coverage (desorbed + reacted) of C_3H_8 σ-complexes (black), and the yield of propane that oxidizes (red) and b) c-C_3H_6 adsorbed on $IrO_2(110)$ at 90 K, including the initial coverage (desorbed + reacted) of c-C_3H_6 σ-complexes (black), and the yield of cyclopropane that oxidizes (red). Blue symbols represent the total, initial propane coverages.

Our results show that both propane compounds are highly reactive on $IrO_2(110)$ at low coverages, with ~100% of the adsorbed C_3H_8 or c-C_3H_6 dissociating and extensively oxidizing to CO_x and H_2O at coverages up to nearly 0.20 ML. The oxidized C_3H_8 yield begins to plateau at a value of 0.18 ML as the total propane coverage passes ~0.20 ML (Figure 3a). Our analysis indicates that the coverage of C_3H_8 σ-complexes continues to increase after the oxidized yield plateaus, with the additional σ-complexes desorbing in the C_3H_8 TPRS peak at 205 K. We estimate that C_3H_8 σ-complexes saturate $IrO_2(110)$ at a coverage of 0.25 ML and that about 72% of the complexes (i.e., 0.18 ML) dissociate and oxidize during TPRS when the σ-complex state is saturated. Further increases in the propane coverage cause C_3H_8 to populate a more weakly-bound state(s) and desorb in a TPRS peak at ~140 K (Figure 1b).

Compared with C_3H_8, a larger quantity of c-C_3H_6 oxidizes on $IrO_2(110)$ during TPRS with increasing propane coverage. Our analysis reveals that the oxidized yield of c-C_3H_6 continues to increase beyond 0.20 ML and saturates at a value 0.31 ML (Figure 3b), which is more than 1.7

times larger than the maximum yield of C_3H_8 that oxidizes during TPRS. Our results also suggest that the saturation coverage of c-C_3H_6 σ-complexes is about 20% higher than that of C_3H_8 (~0.31 vs. 0.25 ML), and in close agreement with our prior estimate of ~0.30 ML for C_2H_6 σ-complexes on IrO_2(110).[12] The higher yield of oxidized c-C_3H_6 vs. C_3H_8 may arise partly from the larger amount of c-C_3H_6 σ-complexes that are accommodated on the IrO_2(110) surface. Additionally, we speculate that ring-opening enables the c-C_3H_6 complexes to form strongly-bound intermediates up to high c-C_3H_6 and HO_{br} coverages, and subsequently oxidize at higher temperature. More specifically, we assert that dehydrogenation of C_3H_8 σ-complexes discontinues beyond a propane coverage of ~0.18 ML due to deactivation of a large quantity of O_{br} atoms via conversion to HO_{br} groups. We expect that dehydrogenation of c-C_3H_6 σ-complexes also ceases beyond a critical c-C_3H_6 coverage, and thus HO_{br} coverage, but that ring-opening occurs in parallel and produces a strongly-bound C_3H_6 intermediate that remains stable to the onset temperature (>~ 400 K) for HO_{br} recombination and thus regeneration of O_{br} atoms, at which point the C_3H_6 intermediate undergoes dehydrogenation and oxidation to CO_x.

Effect of hydrogen pre-coverage

Figures 4a and 4b compare propane and CO_2 TPRS data obtained after exposing as-prepared vs. hydrogen pre-saturated IrO_2(110) surfaces to (nominal) saturation doses of C_3H_8 and c-C_3H_6, respectively. We prepared the H pre-saturated surfaces by first adsorbing H_2 to saturation at 90 K, followed by heating to 380 K to promote H-atom migration from Ir_{cus} to O_{br} atoms. We estimate that the pre-hydrogenation procedure generated ~1.3 ML of H-atoms on the surface, with about 0.80 ML adsorbed on the O_{br} atoms and 0.50 ML on Ir_{cus} atoms (see the Experimental Details

section). As expected, we find that pre-hydrogenating the surface reduces the quantity of both C_3H_8 and c-C_3H_6 that reacts during TPRS, while causing the quantity of propane desorbing at low temperature to increase. We estimate that the oxidized yield of C_3H_8 decreases from 0.17 to ~0.02 ML upon pre-saturating with hydrogen, while the oxidized yield of c-C_3H_6 decreases from 0.33 to 0.17 ML.

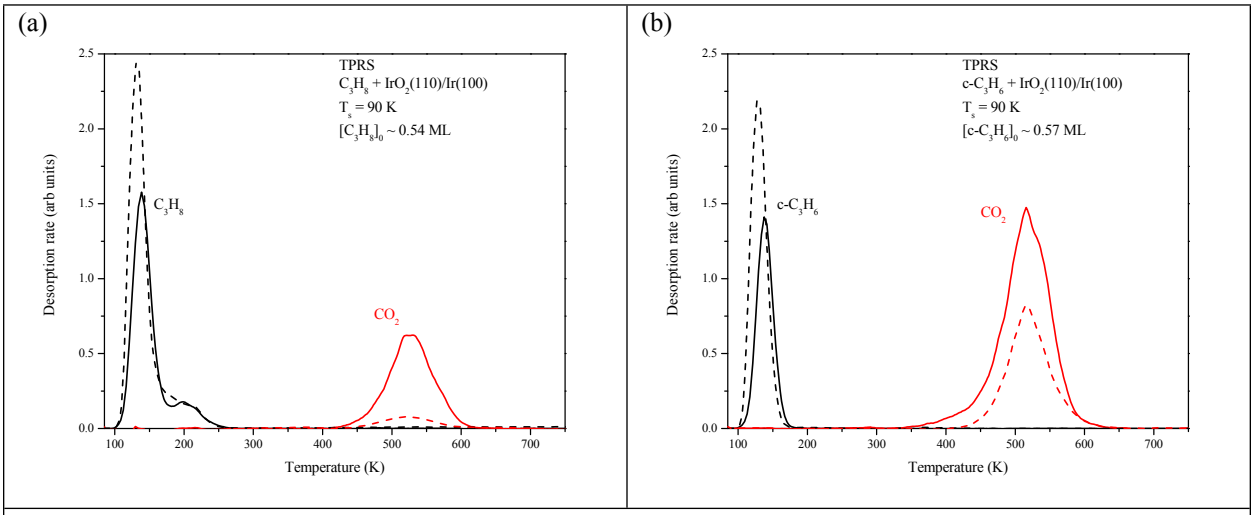

Figure 4: TPRS spectra of (a) C_3H_8 and CO_2 and (b) c-C_3H_6 and CO_2 after adsorbing about 0.54 and 0.57 ML of C_3H_8 or c-C_3H_6 respectively on as-prepared (solid lines) vs. H pre-saturated (dashed lines) IrO_2(110) at 90 K.

Site blocking by H-atoms likely contributes to lowering the quantity of C_3H_8 and c-C_3H_6 that oxidizes on IrO_2(110) after pre-saturating with hydrogen. About 0.5 ML of H-atoms occupy Ir_{cus} sites on the H pre-saturated surfaces and may hinder σ-complex formation during propane adsorption. Such site blocking would lower the initial coverage of C_3H_8 and c-C_3H_6 σ-complexes, and thus the amount of propane that is available to react on the H pre-saturated surfaces. However, our results also demonstrate that a large quantity of c-C_3H_6 activates and oxidizes at HO_{br} coverages that are high enough to nearly completely suppress C_3H_8 activation. Such behavior is consistent with the idea that C_3H_8 dehydrogenation only occurs when O_{br} atoms are available, whereas c-C_3H_6 activation can occur by either dehydrogenation or ring-opening on the Ir_{cus} rows.

Ring-opening should be only weakly dependent on the O_{br} coverage and thus allow c-C_3H_6 activation to occur up to high HO_{br} coverages. Notably, our results show that about the same quantity of C_3H_8 desorbs from the σ-complex state for the clean vs. H pre-saturated IrO_2(110) surfaces, whereas the quantity that reacts is significantly lower on the H-covered surface (Figure 4a). This behavior is consistent with the interpretation that H-atoms on Ir_{cus} sites lower the total quantity of C_3H_8 σ-complexes that form, while HO_{br} groups causes an increase in the fraction of these complexes which desorb. We plan additional studies to more fully characterize how the initial quantity and distribution of H-atoms between the Ir_{cus} and O_{br} atoms influences the formation and activation of propane σ-complexes on IrO_2(110).

Computational Results

C_3H_8 and c-C_3H_6 σ-complexes on IrO_2(110)

We performed DFT-D3 calculations to investigate the adsorption and initial reactions of C_3H_8 and c-C_3H_6 on IrO_2(110). Our calculations predict that both propane compounds initially adsorb on the Ir_{cus} rows and form strongly-bound σ-complexes. Figures 5a and 5b show the most stable configurations that we identified for C_3H_8 and c-C_3H_6 σ-complexes on IrO_2(110) at low coverage. The favored propane σ-complexes have binding energies that are ~30 kJ/mol higher than the second most stable configurations that we identified with DFT-D3 (see SI).

Propane preferentially bonds in a bidentate geometry on IrO_2(110) in which each CH_3 group forms a single η^1 H-Ir dative bond with an Ir_{cus} atom, and the molecular plane is tilted slightly from the surface normal to optimize the H-Ir_{cus} bonding (Figure 5a). Following prior work,[22, 24-26]

we designate this configuration as a p-2η^1 complex where "p" refers to the coordination of only primary C-H bonds with Ir atoms and 2η^1 indicates that the complex forms two η^1 H-Ir bonds. The DFT-D3 calculations predict a binding energy of 145 kJ/mol for the C_3H_8 p-2η^1 complex on IrO_2(110). We have previously found that C_3H_8 binds in the p-2η^1 geometry on PdO(101) and RuO_2(110) but predict lower binding energies of the propane complex on theses surfaces compared with IrO_2(110).[22, 25] Cyclopropane also preferentially forms a 2η^1 complex on IrO_2(110) (Figure 5b), with a computed binding energy of 126 kJ/mol. The molecular geometry allows the C_3H_8 p-2η^1 complex to adopt a more favorable position for H-Ir dative bonding than the c-C_3H_6 complex, and results in a higher binding energy (145 vs. 126 kJ/mol).

PBE-D3 predicts stronger binding of the C_3H_8 σ-complex compared with the desorption energy estimated for the C_3H_8 TPRS peak at 205 K. We note, however, that substantial propane desorption begins to occur experimentally only at propane coverages greater than ~0.20 ML. As discussed in the next section, the C-H bond cleavage barrier is substantially lower than the PBE-D3 desorption energies for both C_3H_8 and c-C_3H_6. Therefore, the isolated propane σ-complexes shown in Fig. 5 will react rather than desorb during the TPRS experiments, and C_3H_8 desorption should only occur at higher coverages when a large fraction of the O_{br} atoms have been hydrogenated and thus deactivated as H-acceptors. We thus assert that the observed C_3H_8 TPRS peak at 205 K arises from C_3H_8 σ-complexes that are adsorbed next to HO_{br} species, and that the neighboring HO_{br} groups weaken the C_3H_8 binding to the surface. Consistent with this assertion, we have recently reported DFT results which show that neighboring HO_{br} groups significantly weaken the binding of an H_2 and C_2H_6 σ-complex on IrO_2(110).[12, 13] We plan a future study to

detail the effects of HO_{br} groups on the binding of alkane σ-complexes on $IrO_2(110)$ but contend that such an effort lies outside of the scope of the present study.

a)	b)
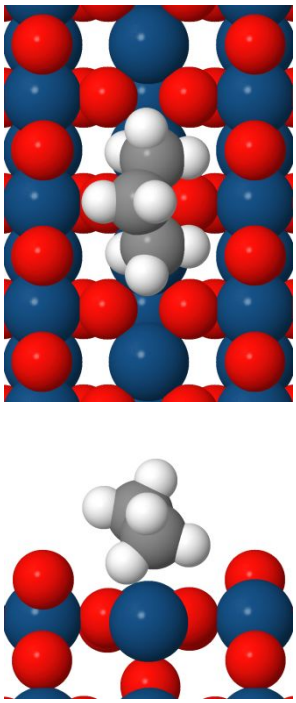	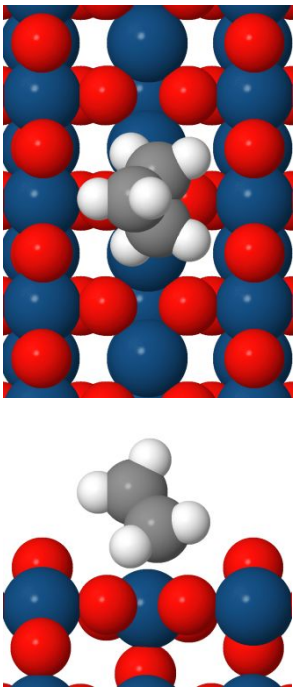
E_b = 145 kJ/mol	E_b = 126 kJ/mol

Figure 5: Molecular configurations of the stable (a) C_3H_8 p-2η^1 complex and (b) c-C_3H_6 2η^1 complex on $IrO_2(110)$ as determined using DFT-D3.

Initial reaction pathways of C_3H_8 on $IrO_2(110)$

Figure 6 shows the energetically-preferred pathway for the initial dehydrogenation of C_3H_8 on $IrO_2(110)$ determined from DFT-D3 calculations as well as the thermochemical barrier for gaseous propylene generation. Our calculations predict a barrier of only 31 kJ/mol and an exothermicity of 99 kJ/mol for initial C-H bond cleavage of the C_3H_8 p-2η^1 complex on $IrO_2(110)$, with reaction occurring by H-transfer to an O_{br} atom to produce an adsorbed C_3H_7 species and an HO_{br} group. Consistent with our experimental findings, the calculations indicate that initial C-H bond activation of the C_3H_8 p-2η^1 complex is strongly favored over C_3H_8 desorption when O_{br} atoms are available

(e.g., low propane coverage) because the barriers for these reactions are 31 vs. 145 kJ/mol, respectively. We find that C-H bond cleavage of the CH_3 group is the energetically preferred step for dehydrogenation of the C_3H_7(ad) species, and generates a stable, bidentate metallacycle of the form Ir-$CH_2CH_2CH_2$-Ir on the Ir_{cus} row. This dehydrogenation reaction features a barrier of 41 kJ/mol and is exothermic by 89 kJ/mol. We compare the C-H bond cleavage pathways of each of the CH_x groups of the C_3H_7(ad) species in the SI.

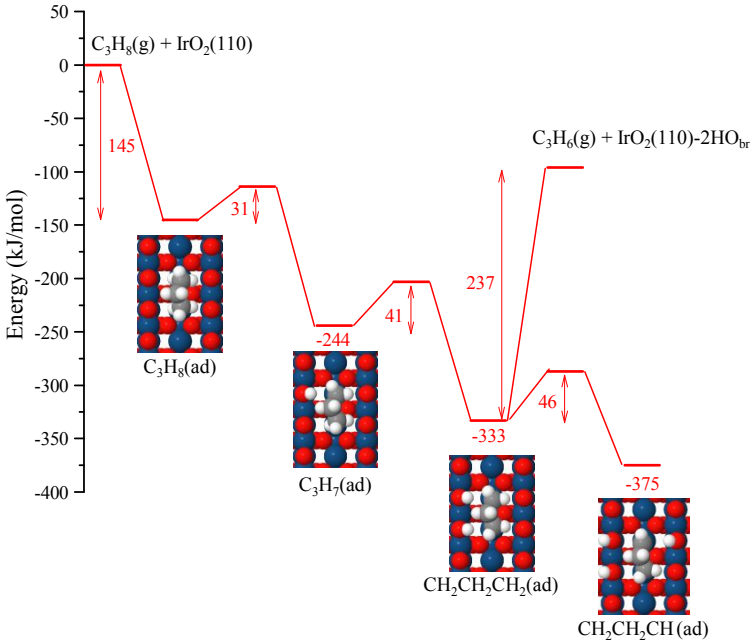

Figure 6: Favored pathway for initial dehydrogenation of C_3H_8 on IrO_2(110) determined from DFT-D3 calculations. Also shown is the energy level of gaseous propylene + the IrO_2(110)-2HO_{br} surface.

Further dehydrogenation of the $CH_2CH_2CH_2$(ad) species is favored over propylene desorption when O_{br} atoms are available. Our calculations predict a barrier of 46 kJ/mol for $CH_2CH_2CH_2$(ad) dehydrogenation via H-transfer to an O_{br} atom, whereas the thermochemical barrier for gaseous C_3H_6 production is 237 kJ/mol (Figure 6). In a previous study of ethane dehydrogenation on IrO_2(110), we showed that HO_{br} groups are ineffective as H-atom acceptors and that ethylene desorption consequently becomes favorable when all of the neighboring O_{br} atoms are

hydrogenated to HO_{br}.[12] In that case, the adsorbed ethylene must overcome a barrier of ~185 kJ/mol to desorb whereas the barriers for HO_{br} recombination and regeneration of O_{br} atoms lie in a range of 220 – 260 kJ/mol.[13] Ethylene is therefore able to desorb at appreciable rates at temperatures lower than that for HO_{br} recombination and H_2O desorption, i.e., <~ 400 K. The situation is different for propane because the thermochemical barrier for C_3H_6(g) evolution lies within the range of barriers for HO_{br} recombination. This result suggests that O_{br} atoms become available at temperatures below that needed for the $CH_2CH_2CH_2$(ad) species to transform and evolve as propylene. The newly-regenerated O_{br} atoms will then promote further dehydrogenation of the $CH_2CH_2CH_2$(ad) species and ultimately extensive oxidation to CO_x, rather than the production of gaseous propylene. An interesting possibility is that propane conversion to propylene could become favored on IrO_2(110) if one can identify an approach for suppressing O_{br} regeneration or acccess of the hydrocarbon intermediate(s) to O_{br} atoms, such as through modification of the oxide structure and composition.

Initial reaction pathways of c-C_3H_6 on IrO_2(110)

Using DFT-D3 we identified two facile pathways for the initial activation of the c-C_3H_6 $2\eta^1$ complex on IrO_2(110) and subsequent dehydrogenation. Figure 7a shows a pathway for sequential dehydrogenation that initiates from C-H bond cleavage of the c-C_3H_6 $2\eta^1$ complex to generate a c-C_3H_5(ad) species and a HO_{br} group. We omitted ring-opening reactions in our analysis of this pathway to maintain computational tractability. The calculations predict that initial dehydrogenation is strongly favored over c-C_3H_6 desorption when O_{br} atoms are available (e.g., low c-C_3H_6 coverage) because the barrier for dehydrogenation is significantly lower than that for

c-C_3H_6 desorption (46 vs. 126 kJ/mol). We find that subsequent dehydrogenation steps involving H-transfer to O_{br} atoms also feature low barriers; we compute barriers of 62 and 77 kJ/mol for the sequential dehydrogenation of c-C_3H_5(ad) and c-C_3H_4(ad), respectively. As expected, the generation of gaseous c-C_3H_4 (cyclopropene) is energetically prohibitive, with a thermochemical barrier (282 kJ/mol) that lies well above the barriers for HO_{br} recombination (~220-260 kJ/mol). The calculations thus suggest that c-C_3H_6 will undergo extensive dehydrogenation and ultimately oxidation on IrO_2(110), after initial C-H activation of the c-C_3H_6 complex. It is worth noting that the barriers for dehydrogenation of the cyclic intermediates resulting from c-C_3H_6, are generally larger than those for dehydrogenation of the C_3H_8-derived intermediates (Figures 6 and 7a), possibly due to increased ring strain upon successive dehydrogenation steps. An implication is that ring-opening is likely to generate more stable, adsorbed species for which dehydrogenation is even more facile than predicted for the cyclic intermediates.

We find that the c-C_3H_6 $2\eta^1$ complex can also undergo ring-opening on IrO_2(110), followed by facile dehydrogenation (Figure 7b). Ring-opening of the c-C_3H_6 complex produces a bidentate Ir-$CH_2CH_2CH_2$-Ir species that is nominally the same structure as that resulting from C_3H_7(ad) dehydrogenation (Figure 6). The ring-opening reaction is more exothermic than C-H bond cleavage of the c-C_3H_6 complex (134 vs. 89 kJ/mol) but has a larger barrier (61 vs. 46 kJ/mol), indicating that c-C_3H_6 will preferentially react by C-H bond cleavage rather than ring-opening when O_{br} atoms are available. Sequential dehydrogenation of the C_3H_6(ad) species via H-transfer to O_{br} atoms is also facile and exothermic, with barriers of 43 and 59 kJ/mol for the consecutive steps that generate C_3H_4(ad) (Figure 7b).

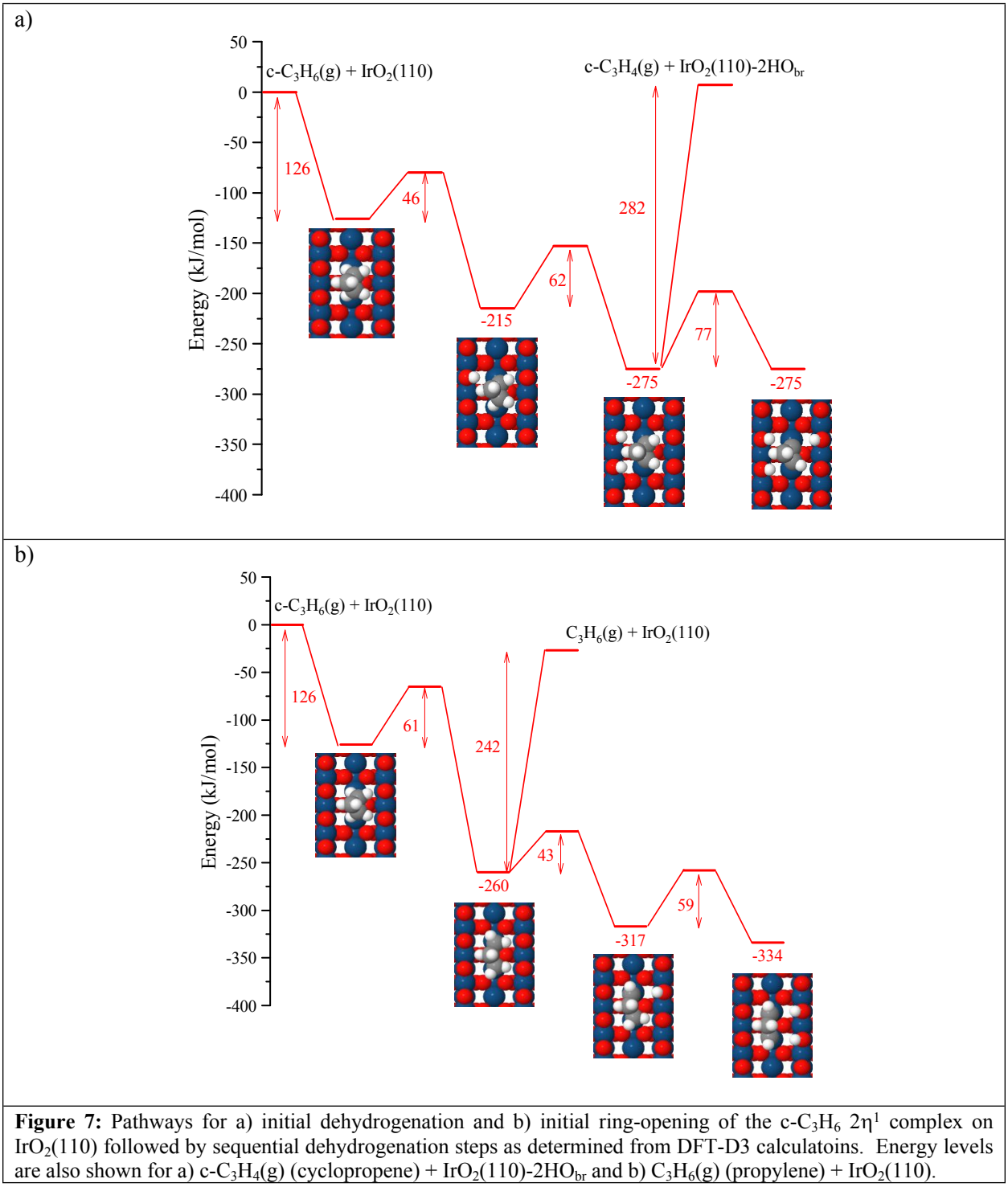

Figure 7: Pathways for a) initial dehydrogenation and b) initial ring-opening of the c-C_3H_6 $2\eta^1$ complex on $IrO_2(110)$ followed by sequential dehydrogenation steps as determined from DFT-D3 calculatoins. Energy levels are also shown for a) c-C_3H_4(g) (cyclopropene) + $IrO_2(110)$-$2HO_{br}$ and b) C_3H_6(g) (propylene) + $IrO_2(110)$.

The ability of the c-C_3H_6 complex to undergo ring-opening and generate a stable C_3H_6(ad) intermediate can qualitatively explain our experimental finding that larger quantities of c-C_3H_6 react on IrO_2(110) compared with C_3H_8. Because facile activation of C_3H_8 σ-complexes requires O_{br} atoms, the yield of reacted C_3H_8 reaches a limit once a sufficient amount of O_{br} atoms have converted to HO_{br}, at which point additional C_3H_8 complexes desorb during TPRS. In contrast, ring-opening is nearly independent of the O_{br} coverage and can thus generate a stable intermediate at high HO_{br} coverages. We note that the binding energy of the bidentate C_3H_6(ad) species and barrier for C-H bond cleavage via H-transfer to an O_{br} atom are only weakly dependent on the local HO_{br} coverage. The thermochemical barriers for the C_3H_6(ad) species to evolve as gaseous propylene or cyclopropane are also greater than those for HO_{br} recombination and O_{br} regeneration. Thus, unlike the C_3H_8 σ-complex, our calculations predict that the C_3H_6(ad) species will remain adsorbed to temperatures beyond the onset for O_{br} regeneration, at which point dehydrogenation and extensive oxidation will ensue. The possibility for initial ring-opening in addition to dehydrogenation thus allows a larger quantity of c-C_3H_6 to extensively oxidize on IrO_2(110) compared with C_3H_8, in agreement with our experimental findings.

Summary

We investigated the adsorption and oxidation of C_3H_8 and c-C_3H_6 on IrO_2(110) using TPRS and DFT calculations. We find that the activation of both C_3H_8 and c-C_3H_6 is facile on IrO_2(110) and that the dissociated alkanes subsequently oxidize to CO, CO_2 and H_2O during TPRS above 400 K. We observe negligible propylene evolution under the conditions studied. Our results show that nearly all of the adsorbed C_3H_8 and c-C_3H_6 oxidize on IrO_2(110) at low coverage, and that the

yield of oxidized propane rises to a plateau with increasing propane coverage. We find that the maximum yield of propane that oxidizes is higher for c-C_3H_6 compared with C_3H_8 (~0.30 vs. 0.18 ML), and that pre-saturating the IrO_2(110) surface with hydrogen suppresses the reactivity of C_3H_8 almost completely, whereas a large quantity of c-C_3H_6 oxidizes on the pre-hydrogenated surface.

Our DFT-D3 calculations predict that C_3H_8 and c-C_3H_6 form strongly-bound σ-complexes on IrO_2(110) and that initial C-H bond cleavage as well as subsequent dehydrogenation is highly facile via H-transfer to O_{br} atoms. We predict that sequential dehydrogenation of C_3H_8 preferentially generates a bidentate C_3H_6 species on the Ir_{cus} rows, and that the barrier for the C_3H_6 species to transform to propylene and desorb is higher than that for O_{br} regeneration by HO_{br} recombination. The calculations thus suggest that propane conversion to propylene is negligible on IrO_2(110) because O_{br} atoms become available and promote further dehydrogenation at temperatures below those needed for appreciable propylene desorption. We predict that initial activation of the c-C_3H_6 complex can occur by both H-transfer to an O_{br} atom as well as ring-opening on the Ir_{cus} row. The ring-opening reaction allows c-C_3H_6 to convert to a strongly-bound intermediate at high, initial HO_{br} coverage, and can explain the higher reaction yields that we observe during TPRS for c-C_3H_6 compared with C_3H_8 on the as-prepared and pre-hydrogenated IrO_2(110) surface.

Supporting Information

Structure of the s-IrO_2(110) layer on Ir(100); Measurement of product yields; TPRS traces for C_3H_8 as a function of coverage on IrO_2(110); TPRS traces for c-C_3H_6 as a function of coverage on IrO_2(110); Configurations of C_3H_8 σ-complexes on IrO_2(110) predicted by DFT-D3;

Configurations of c-C_3H_6 σ-complexes on IrO_2(110) predicted by DFT-D3; Pathways for dehydrogenation of different CH_x groups of adsorbed propyl (C_3H_7) on IrO_2(110).

Acknowledgements

We acknowledge the Ohio Supercomputing Center for providing computational resources. We gratefully acknowledge financial support for this work provided by the Department of Energy, Office of Basic Energy Sciences, Catalysis Science Division through Grant DE-FG02-03ER15478.

References

1. C. A. Gartner, A. C. van Veen and J. A. Lercher, *Chemcatchem*, 2013, 5, 3196-3217.
2. F. Cavani, N. Ballarini and A. Cericola, *Catal. Today*, 2007, 127, 113-131.
3. M. A. Banares, *Catal. Today*, 1999, 51, 319-348.
4. C. A. Gartner, A. C. van Veen and J. A. Lercher, *J. Am. Chem. Soc.*, 2014, 136, 12691-12701.
5. M. D. Argyle, K. D. Chen, A. T. Bell and E. Iglesia, *J. Catal.*, 2002, 208, 139-149.
6. M. D. Argyle, K. D. Chen, A. T. Bell and E. Iglesia, *J. Phys. Chem. B*, 2002, 106, 5421-5427.
7. M. V. Martinez-Huerta, X. Gao, H. Tian, I. E. Wachs, J. L. G. Fierro and M. A. Banares, *Catal. Today*, 2006, 118, 279-287.
8. X. Rozanska, R. Fortrie and J. Sauer, *J. Am. Chem. Soc.*, 2014, 136, 7751-7761.
9. C. A. Carrero, R. Schloegl, I. E. Wachs and R. Schomaecker, *ACS Catal*, 2014, 4, 3357-3380.
10. X. P. Wu and X. Q. Gong, *J. Am. Chem. Soc.*, 2015, 137, 13228-13231.
11. Z. Liang, T. Li, M. Kim, A. Asthagiri and J. F. Weaver, *Science*, 2017, 356, 298-301.
12. Y. X. Bian, M. Kim, T. Li, A. Asthagiri and J. F. Weaver, *J. Am. Chem. Soc.*, 2018, 140, 2665-2672.
13. T. Li, M. Kim, Z. Liang, A. Asthagiri and J. F. Weaver, *Top. Catal.*, 2018, 61, 397-411.
14. P. E. Blochl, *Phys. Rev. B*, 1994, 50, 17953-17979.
15. G. Kresse and J. Hafner, *J. Non-Cryst. Solids*, 1993, 156, 956-960.

16. G. Kresse, *J. Non-Cryst. Solids*, 1995, 193, 222-229.

17. J. P. Perdew, K. Burke and M. Ernzerhof, *Phys. Rev. Lett.*, 1996, 77, 3865-3868.

18. S. Grimme, J. Antony, S. Ehrlich and H. Krieg, *J. Chem. Phys.*, 2010, 132, 154104.

19. G. Henkelman, B. P. Uberuaga and H. Jonsson, *J. Chem. Phys.*, 2000, 113, 9901-9904.

20. S. L. Tait, Z. Dohnalek, C. T. Campbell and B. D. Kay, *J. Chem. Phys.*, 2006, 125, 234308.

21. L. Chen, R. S. Smith, B. D. Kay and Z. Dohnalek, *Surf. Sci.*, 2016, 650, 83-92.

22. T. Li, M. Kim, R. Rai, Z. Liang, A. Asthagiri and J. F. Weaver, *Phys. Chem. Chem. Phys.*, 2016, 18, 22647-22660.

23. T. Li, R. Rai, Z. Liang, M. Kim, A. Asthagiri and J. F. Weaver, *J. Phys. Chem. C*, 2016, 120, 9863-9873.

24. A. Antony, A. Asthagiri and J. F. Weaver, *Phys. Chem. Chem. Phys.*, 2012, 14, 12202-12212.

25. A. Antony, C. Hakanoglu, A. Asthagiri and J. F. Weaver, *J. Chem. Phys.*, 2012, 136, 054702.

26. F. Zhang, L. Pan, J. Choi, V. Mehar, J. T. Diulus, A. Asthagiri and J. F. Weaver, *Angew. Chem., Int. Ed.*, 2015, 54, 13907-13911.